scientific reports

Check for updates

OPEN

The role and function validation of P2RX4 as a novel cancer biomarker in pan-cancer analysis

Xiaoyuan Qiao[1], Chunyan Wang[2] & Jun Ma[3]✉

Purinergic Receptor P2X4 (P2RX4) is implicated in the carcinogenesis of several cancers, but no extensive study on its role in different forms of cancer. Expression level, gene mutation, immune infiltration, pathway enrichment, and prognostic value analysis of P2RX4 were performed based on multiple publicly available databases such as TCGA, GTEx, GEO, TIMER2, cBioportal, and Metascape databases. Western blot and RT-qPCR were used to identify P2RX4 expression in liver hepatocellular carcinoma (LIHC) and paracancer samples. P2RX4 was knocked in glioblastoma cell line (U251) and prostate cancer cell line (PC3), and its effects on cell viability, apoptosis, migration and invasion were investigated through cell counting kit-8 assay, flow cytometry, wound healing and trasnwell assays, respectively. P2RX4 expression was elevated in most cancers, which predicted poor overall survival and disease-free survival. Mutations in P2RX4 were predominantly found in Lymphoid Neoplasm Diffuse Large B-cell Lymphoma (> 4%). P2RX4 expression showed a positive correlation with the infiltration levels of cancer-associated fibroblasts and CD8 + cells in multiple tumor types. Functional enrichment analysis indicated that P2RX4 is closely related to autophagy, protein modification or intracellular trafficking. P2RX4 was highly expressed in LIHC compared to paracancerous tissues. Knockdown of P2RX4 suppressed cell viability, migration, invasion, and promoted cell apoptosis of U251 and PC3 cells. Overexpression of P2RX4 occurred in multi cancers, and was connected to an unfavorable prognosis. This pan-cancer analysis highlighted the predictive value and tumorigenic role of P2RX4.

Keywords Biomarker, P2RX4, Immune infiltration, Prognosis, Pan-cancer

Cancer is the main cause of sickness and mortality worldwide, with enormous health and economic consequences for society[1]. As per the "Global cancer statistics 2022" report, cancer has led to 9.7 million deaths, with nearly 20 million new cases confirmed worldwide[2]. Despite advancements in multimodal therapies—including targeted therapies and immunotherapies—the heterogeneity of tumors and the emergence of treatment resistance continue to limit clinical outcomes[3]. Early diagnosis and precision medicine are critical for improving patient survival, yet the lack of robust biomarkers with broad applicability across cancer types remains a significant challenge[4]. Given the complexity of carcinogenesis, it is required to undertake a pan-cancer expression research of any potential gene, examine its connection to clinical outcome, and investigate probable molecular explanations[5].

Purinergic Receptor P2X 4 (P2RX4), an ATP-gated ion channel, is increasingly recognized for its multifaceted roles in biological processes, including inflammatory pain[6], neuropathic pain following nerve damage[7,8], T-cell migration[9], and cardiac function[10]. P2RX4 is also implicated in activated microglia survival, as well as memory issues in in type 2 diabetic rats[11]. Recent studies underscore its oncogenic potential. In prostate cancer, the pharmacological inhibition of P2RX4 curtails tumor growth and metastasis[12]. Significantly, P2RX4-mediated ATP signaling is involved in T-cell migration[9], while it propels mammary cancer progression by sustaining autophagy and related mesenchymal transition in breast cancer (BRCA)[13]. However, existing research is fragmented, focusing on isolated cancer types without systematic exploration of its pan-cancer expression patterns, prognostic significance, or immune interactions. A comprehensive analysis of P2RX4 across multi cancers is lacking, leaving critical gaps in understanding its universal versus context-dependent roles.

Pan-cancer analysis is indispensable for understanding the environmental dependence of gene functions. It detects prevalent expression patterns and mutational landscapes, reveals common features of immune cell

[1]Department of Comprehensive Medicine, Cancer Hospital Affiliated to Shanxi Medical University, Shanxi Hospital Affiliated to Cancer Hospital Chinese Academy of Medical Sciences, Taiyuan, China. [2]Department of Laboratory Medicine, Cancer Hospital, Shanxi Cancer Hospital, Shanxi Medical University, Shanxi Hospital Affiliated to Cancer Hospital Chinese Academy of Medical Sciences, Taiyuan, China. [3]Department of General Surgery, Cancer Hospital Affiliated to Shanxi Medical University, Shanxi Hospital Affiliated to Cancer Hospital Chinese Academy of Medical Sciences, No. 3 Zhigong New Street, Taiyuan 030013, Shanxi, China. ✉email: Mjsxszlyy@163.com

infiltration in the tumor microenvironment, and provides evidence for optimizing immunotherapy strategies[14]. Integrating multi-omics data (such as transcriptomic, proteomic, and immune profiling information) can clarify shared molecular pathways like autophagy or immune infiltration, guiding precision medicine and drug development[15]. Furthermore, pan-cancer analysis, by integrating epigenetic and metabolomic data, develops early diagnostic biomarkers and prognostic models for multiple cancer types[16]. In this study, we conducted the first comprehensive pan-cancer investigation of P2RX4, analyzing its expression, prognostic relevance, genetic alterations, immune interactions, and functional networks across 33 tumor types. Our findings position P2RX4 as a potential pan-cancer biomarker and therapeutic target, offering insights into its mechanistic contributions to tumorigenesis and immune modulation.

Materials and methods

P2RX4 expression analysis

P2RX4 was imported into the 'Gene DE' module of the Tumor Immune Estimation Resource (TIMER2, version 2.0, http://timer.cistrome.org/)[17], and P2RX4 expression in The Cancer Genome Atlas database (TCGA; https://www.cancer.gov/ccg/research/genome-sequencing/tcga) was compared between 33 types (Table 1) tumor and surrounding normal tissues for various cancers and tumor subtypes. For some tumors with no or limited normal tissue (such as TCGA-adrenocortical carcinoma (ACC) and TCGA-skin cutaneous melanoma (SKCM)), differential expression analyses were performed using the Gene Expression Profiling Interactive Analysis 2 (GEPIA2, http://gepia2.cancer-pku.cn/#analysis)[18] with a p-value cutoff of 0.01, a $\log_2$foldchange cutoff of 1, and the 'Match TCGA normal and GTEx data' option was selected.

The protein expression analysis of the CPTAC dataset were conducted by employing the UALCAN portal (http://ualcan.path.uab.edu/analysis-prot.html), an interactive online resource for cancer Omics data[19]. By choosing 'P2RX4', we investigated the P2RX4 protein levels in cancers and normal tissues. Six cancer-related

Abbreviation	Full name
ACC	Adrenocortical carcinoma
BLCA	Bladder Urothelial Carcinoma
BRCA	Breast invasive carcinoma
CESC	Cervical squamous cell carcinoma and endocervical adenocarcinoma
CHOL	Cholangiocarcinoma
COAD	Colon adenocarcinoma
DLBC	Lymphoid neoplasm diffuse large B-cell lymphoma
ESCA	Esophageal carcinoma
GBM	Glioblastoma multiforme
HNSC	Head and neck squamous cell carcinoma
KICH	Kidney chromophobe
KIRC	Kidney renal clear cell carcinoma
KIRP	Kidney renal papillary cell carcinoma
LAML	Acute myeloid leukemia
LGG	Brain lower grade glioma
LIHC	Liver hepatocellular carcinoma
LUAD	Lung adenocarcinoma
LUSC	Lung squamous cell carcinoma
MESO	Mesothelioma
OV	Ovarian serous cystadenocarcinoma
PAAD	Pancreatic adenocarcinoma
PCPG	Pheochromocytoma and paraganglioma
PRAD	Prostate adenocarcinoma
READ	Rectum adenocarcinoma
SARC	Sarcoma
SKCM	Skin cutaneous melanoma
STAD	Stomach adenocarcinoma
TGCT	Testicular germ cell tumors
THCA	Thyroid carcinoma
THYM	Thymoma
UCEC	Uterine corpus endometrial carcinoma
UCS	Uterine carcinosarcoma
UVM	Uveal melanoma

Table 1. 33 Types of tumors in the TCGA database.

datasets were chosen, including BRCA, clear cell renal cell carcinoma (RCC), uterine corpus endometrial carcinoma (UCEC), colon cancer, glioblastoma multiforme (GBM), and liver hepatocellular carcinoma (LIHC).

Immunohistochemistry (IHC) staining data results and IHC pictures of P2RX4 protein level in six tumor tissues and normal tissues, including BRCA, colon adenocarcinoma (COAD), LIHC, UCEC, GBM, and ACC were acquired from the Human Protein Atlas (HPA) database (version 20.1; https://www.proteinatlas.org/)[20]. Moreover, the P2RX4 protein and RNA expression levels were analyzed using 'TISSUE' module in the HPA database. We also developed an expression map of P2RX4 for single cell type in the 'SINGLE CELL' part.

Prognosis analysis

The correlation between P2RX4 expression and overall survival (OS) and disease-free survival (DFS) of 33 tumors was evaluated by the 'GEPIA2 Survival Map' module in the GEPIA2 database[18]. In addition, survival plots were generated using the 'GEPIA2 Survival Analysis' Module. Tumor transcriptome sequencing and control normal data, as well as corresponding clinical information were downloaded from the TCGA and GTEx databases. Receiver operating characteristic (ROC) curves were developed for prognostic analysis using the "Survival ROC" package in R language (version 4.4.2, https://imagej.net/). The diagnostic significance of the area under the ROC curve (AUC), which ranged between 0.5 and 1, and enhanced as the AUC approaches 1. When utilizing the cBioPortal site (version 6.0.25, https://www.cbioportal.org/)[21] for P2RX4 mutation analysis, we investigated the genetic changes of P2RX4 by selecting the 'TCGA Pan Cancer Atlas Studies' and searching for 'P2RX4' in the 'Query by Gene' section. All TCGA Pan-Cancer Atlas studies were included in our research. We used the 'Cancer Type Summary', 'Mutations', and 'mRNA vs Study' modules to obtain genetic alteration data of P2RX4 in the pan-cancer cohort.

Immune infiltration analysis

The 'Immune-Gene' module of the TIMER2 was employed to analyze the correlation between P2RX4 expression and immune cells, including $CD8^+$ T-cells and cancer-associated fibroblasts (CAF). TIMER, CIBERSORT, CIBERSORT-ABS, QUANTISEQ, XCELL, TIDE, MCPCOUNTER, and EPIC algorithms were used to estimate immune infiltration.

P2RX4-related gene enrichment analysis

The 'Similar Gene Detection' module in GEPIA2 was used to retrieve 100 P2RX4-correlated genes. The gene properties of 100 genes were utilized as input gene symbols in Metascape (http://metascape.org)[22] for a Gene Ontology (GO) pathway enrichment analysis. Additionally, the 'Correlation Analysis' module in GEPIA2 was employed to perform pairwise gene regression analysis.

P2RX4-protein interaction analysis

A P2RX4-protein interaction network was constructed using the 'Network' module of BioGRID (version 4.4.242; https://thebiogrid.org/)[23] with the format set to 'Concentric Circles'.

Cell culture

Astrocytes (HEB), glioblastoma cell line (U251), normal prostate cell line (RWPE-1) and prostate cancer cell line (PC3) were purchased from iCell (Shanghai, China). HEB cells were cultured in minimum essential medium supplemented with 10% fetal bovine serum (FBS). U251 cells were maintained in Dulbecco's Modified Eagle Medium containing 10% FBS and 1% penicillin-streptomycin. RWPE-1 cells were grown in keratinocyte serum-free medium, augmented with 0.05 mg/ml bovine pituitary extract and 5 ng/ml human recombinant epidermal growth factor. PC3 cells were cultured in Roswell Park Memorial Institute-1640 medium supplemented with 10% FBS. All cells were placed in the incubator at 37 °C, 5% CO_2. siRNAs targeting P2RX4 (si-P2RX4-1,2,3) were used to silence P2XR4 expression in cells, and non-targeted siRNA (si-NC) was used as a control. siRNAs were transfected into cells using Lipofectamine 3000 (Thermo Fisher Scientific, Waltham, MA, USA), and primer sequences of siRNAs were listed in Table 2.

Primer name	Sequence (5′–3′)
GAPDH-F	GTCAGTGGTGGACCTGACCT
GAPDH-R	TGCTGTAGCCAAATTCGTTG
P2RX4-F	TTGTGTGGGAAAAGGGCTAC
P2RX4-R	CCTGTGTCTGGTTCATGGTG
si-NC-F	UUCUCCGAACGUGUCACGUTT
si-NC-R	ACGUGACACGUUCGGAGAATT
si-P2RX4-F-1	AAAAGAGUGAAGUUUUCUGCA
si-P2RX4-R-1	CAGAAAACUUCACUCUUUUGG
si-P2RX4-F-2	UUGUUCUUAACCAAAAGAGUG
si-P2RX4-R-2	CUCUUUUGGUUAAGAACAACA
si-P2RX4-F-3	UAAGUAGUGGUGAUGUUGGGA
si-P2RX4-R-3	CCAACAUCACCACUACUUACC

Table 2. RT-qPCR primer sequences.

Cell counting kit (CCK)-8 assay
U251 and PC-3 cells (2×10^5/mL) were seeded into 96-well plates and pre-cultured in an incubator (37 °C, 5% CO_2) for 24 h. Cells were then cultured in the incubator for 2 h, and the absorbance at 450 nm was monitored hourly to determine the optimal culture time using a microplate reader.

Wound healing assay
U251 and PC-3 cells were cultured in 6-well plates until reaching full coverage. A sterile pipette tip was used to create linear scratches on the cell layer. Images were captured immediately after scratching and at 24 h post-scratching. Wound closure area was quantified using Image J software (version 1.8.0, https://imagej.nih.gov/ij/) to assess cell migratory ability.

Transwell assay
Cell invasion was evaluated using Matrigel-coated Transwell chambers. Cells (5×10^4/well) were seeded into the upper chambers, while the lower chambers were filled with medium containing 20% FBS as a chemoattractant. After 24 h of incubation at 37 °C, non-invading cells in the upper chambers were removed. Invaded cells in the lower chambers were fixed with 4% paraformaldehyde, stained with 0.1% crystal violet, and counted under a light microscope (Olympus, Tokyo, Japan).

Flow cytometry
Cells went through centrifugation and resuspension. Then, cells were incubated with Annexin V-FITC and propidium iodide solution at room temperature (20–25℃) for 15 min in the dark. The apoptosis of cells was measured by flow cytometry (Cytoflex, BD Biosciences, USA).

Western blot
To detect the P2RX4 protein level, β-actin was utilized as an internal reference control. Proteins were separated by lysis buffer. Subsequently, sodium dodecyl sulfate–polyacrylamide gel electrophoresis was performed for protein electrophoresis. Afterwards, proteins were transferred onto a polyvinylidene fluoride membrane for 2 h at 4 °C. The membrane was then recovered and subjected to blocking with 5% non-fat milk, followed by agitation for 2 h at room temperature. Post-blocking, the membrane was thoroughly rinsed and incubated overnight at 4 °C with primary antibodies (1/1000, Abcam, Cambridge, UK), including P2RX4 (ab243734) and β-actin (ab8227). After rinsing with TBST, the membrane was subsequently probed with goat anti-rabbit IgG secondary antibody (ab150077, Abcam) for 1 h at room temperature. The membrane was slightly blotted with TBST solution on blotting paper and laid on the Tanon 5200 chemiluminescence imaging system incubation plate; enhanced chemiluminescence was developed and exposed for image acquisition.

Enzyme-linked immunosorbent assay (ELISA)
The levels of reactive oxygen species (ROS) in cell supernatants were assessed according to the respective ELISA kit (Esebio, Shanghai, China) instructions. The optical density of samples was measured with a microplate reader, and concentrations were calculated from standard curves.

Real-time quantitative polymerase chain reaction (RT-qPCR)
RNA was extracted from cells using TRIzol reagent. The concentration of RNA was determined by taking 1 μL of RNA on a Nano-100 instrument. cDNA synthesis was done using the SweScript All-in-One First-Stand cDNA Synthesis Supermix for qPCR Reverse Transcription Kit from Service Biotechnology Co. (Wuhan, China). Afterwards, reverse transcription is conducted according to the following reaction conditions: 25 °C, 5 min; 42 °C, 15–30 min; 85 °C, 5 s. The cDNA samples were examined by qPCR using the ChamQ Universal SYBR qPCR Master Mix (Vazyme, Nanjing, China). The reaction conditions were: initial denaturation at 95 °C for 30 s, 40 cycles of 95 °C for 10 s and 60 °C for 30 s, followed by 95 °C for 15 s, 60 °C for 60 s and 95 °C for 15 s. For each gene, primers were designed to measure the mRNA level (Table 2), and GAPDH was set as an internal reference control.

Statistical analysis
All data were meticulously analyzed utilizing GraphPad Prism 9.0 (https://www.graphpad.com/) and presented as mean ± standard deviation. For the comparison between two groups, a t-test was employed, whereas for the evaluation among multiple groups, One-Way ANOVA was utilized. Tukey's test was applied to conduct pairwise comparisons. The $p < 0.05$ was considered statistically significant.

Results
Gene expression analysis
The TIMER2 tool was employed to investigate the status of P2RX4 expression level across various kinds of cancers based on the TCGA database. P2RX4 expression levels were higher in bladder cancer (BLCA), BRCA, cholangio carcinoma (CHOL), esophageal carcinoma (ESCA), GBM, head and neck squamous cell carcinoma (HNSC), HNSC-HPV+ (rectum adenocarcinoma), kidney renal clear cell carcinoma (KIRC), kidney renal papillary cell carcinoma (KIRP), LIHC, lung adenocarcinoma (LUAD), prostate adenocarcinoma (PRAD), stomach adenocarcinoma (STAD), thyroid cancer (THCA), and UCEC tumor tissues than in normal tissues, as displayed in Fig. 1A. The expression of P2RX4, on the other hand, was significantly decreased in COAD, kidney chromophobe (KICH), lung squamous cell carcinoma (LUSC), and rectum adenocarcinoma (READ).

We evaluated expression changes in P2RX4 between normal and malignant tissues for ACC, lymphoid neoplasm diffuse large B-cell lymphoma (DLBC), acute myeloid leukemia (LAML), brain lower grade glioma

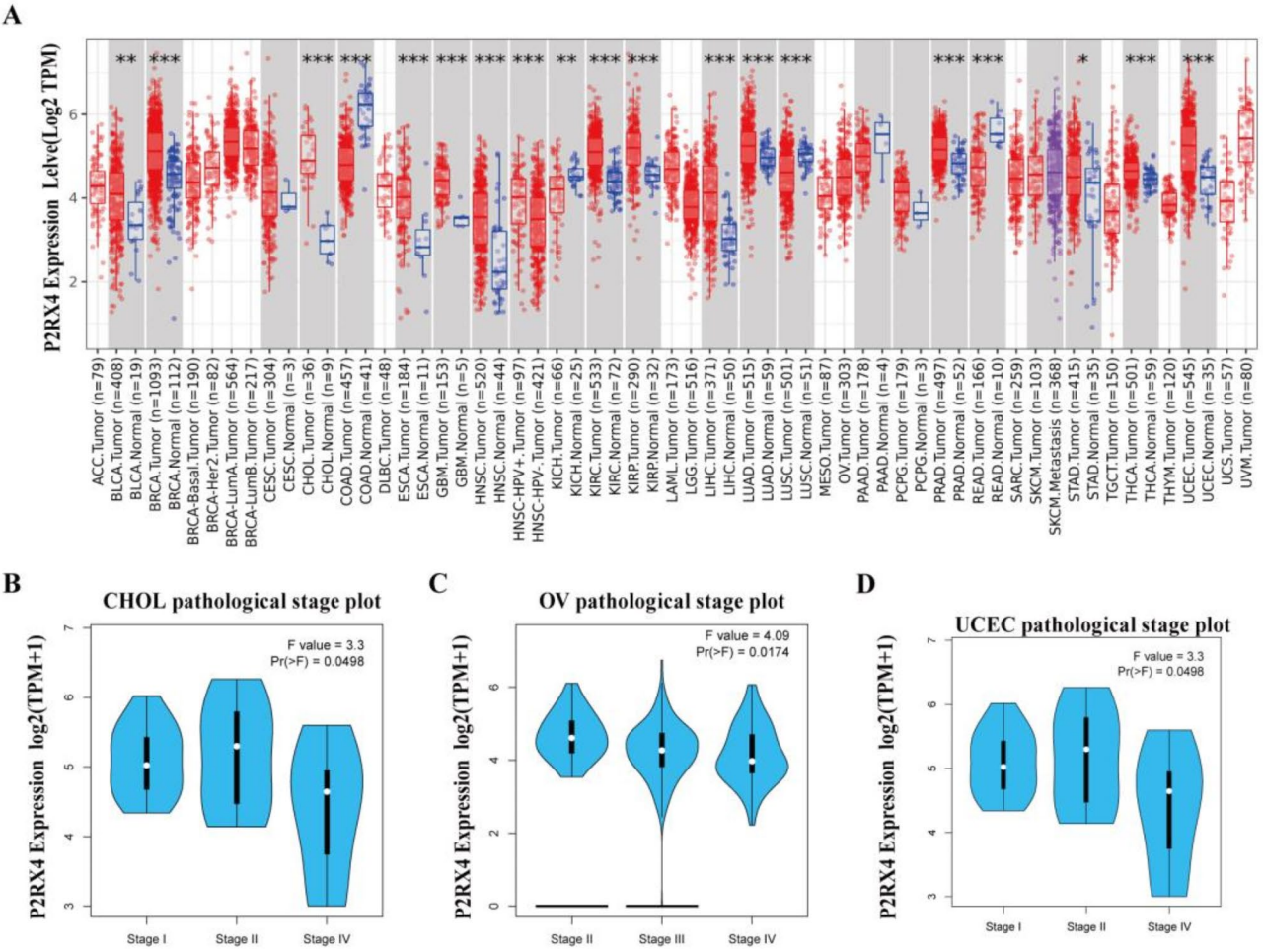

Fig. 1. Purinergic receptor P2X 4 (P2RX4) gene expression levels in various cancers and clinical phases. (**A**) Expression status of the P2RX4 gene in different cancers or specific cancer subtypes analyzed by TIMER2 (*$p < 0.05$; **$p < 0.01$; ***$p < 0.001$). (**B**) Based on TCGA data, the expression levels of the P2RX4 gene were examined in relation to the major pathogenic phases (I, II, III and IV) of Ovarian serous cystadenocarcinoma (OV) and Uterine Corpus Endometrial Carcinoma (UCEC). Log_2 (TPM + 1) was applied for log scaling.

(LGG), ovarian serous cystadenocarcinoma (OV), Sarcoma (SARC), testicular germ cell tumors (TGCT), thymoma (THYM), and uterine carcinosarcoma (UCS) (Supplementary Figure S1), with normal tissues from the GTEx dataset as controls. P2RX4 expression and tumor pathological stages were also investigated using GEPIA2. P2RX4 expression was found to be significantly linked with advanced stages of CHOL, OV, and uterine corpus endometrial carcinoma (UCEC) (Fig. 1B–D).

Protein expression analysis

Based on HPA, GTEx, and FANTOM5 (mammalian genome function annotation) datasets, we discovered that P2RX4 was significantly expressed in the gastrointestinal tract, such as the colon and small intestine, and enriched in the lung, pancreas, placenta, and appendix (Fig. 2A; Figure S2A-2 C). The P2RX4 protein was subsequently investigated and shown to be broadly high expression in a variety of normal tissues (Fig. 2B). These results suggested that P2RX4 expression was ubiquitously observed across different tissues. Also included was a summary of all tissues where single cell type expression has been studied (Fig. 3). Based on these data, P2RX4 single cell type specificity was improved (Syncytiotrophoblasts, Cytotrophoblasts, Hofbauer cells, Proximal enterocytes, Intestinal goblet cells) (Figure S2D).

P2RX4 protein expression was analyzed using IHC results retrieved from the HPA database, comparing it with TCGA data on P2RX4 gene expression. Consistent trends in the two databases were observed, as shown in Figs. 2C-H. The IHC staining for P2RX4 was robust in normal colon tissues but weak in tumor tissues. P2RX4 staining was modest in normal renal endometrial and liver tissue samples, but strong in malignant tissue samples. Furthermore, P2RX4 expression is low in the cerebral cortex but considerable in GBM. P2RX4 staining was absent in normal breast tissues, but moderate in BRCA. P2RX4 protein levels were greater in primary BRCA, KIRC, GBM, LIHC, and UCEC tissues than in normal tissues (Fig. 2I, $p < 0.005$). P2RX4 expression, on the other hand, was drastically decreased in colon cancer (Fig. 2I, $p < 0.001$).

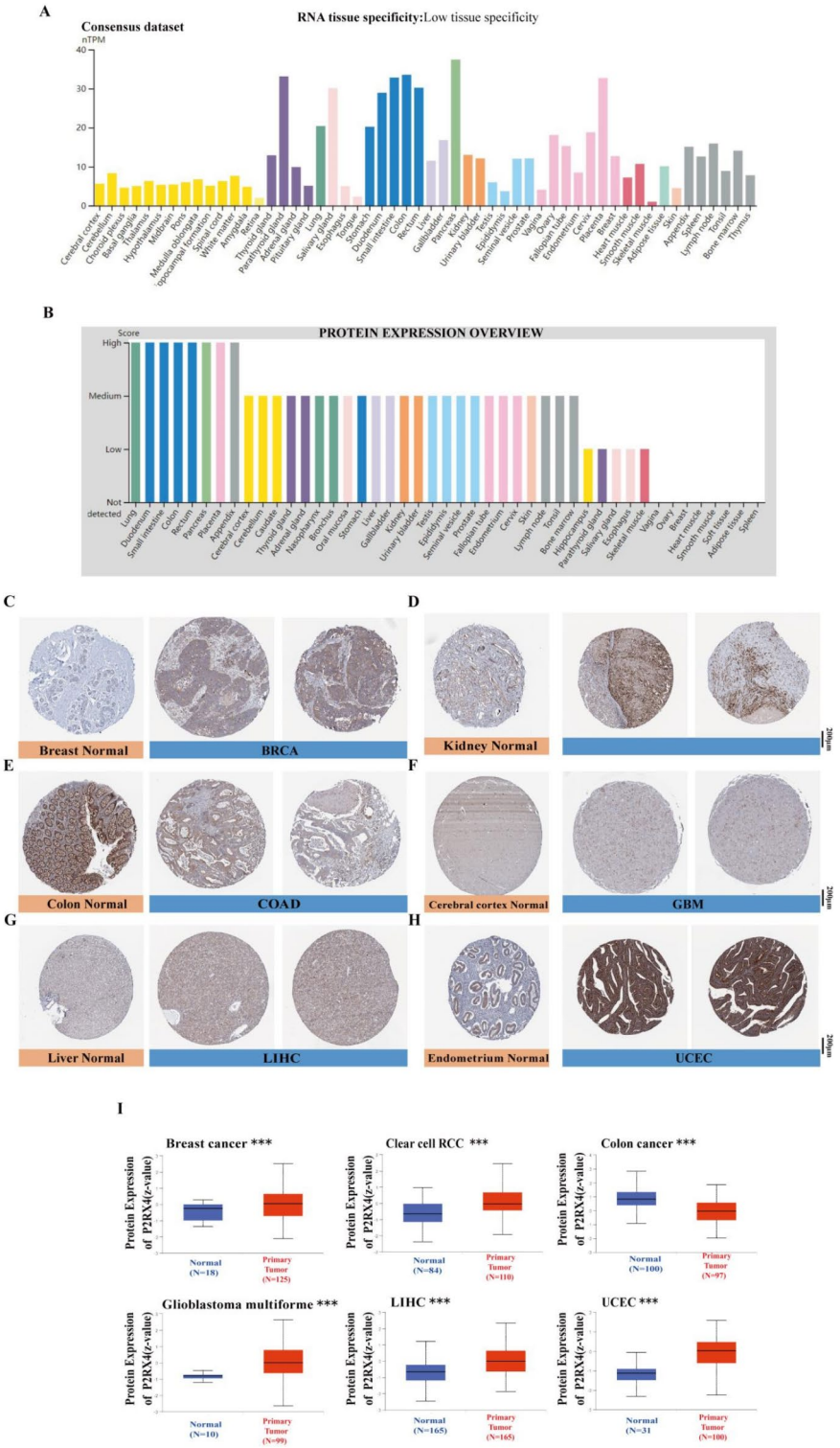

Fig. 2. P2RX4 expression patterns in normal and cancerous tissues in humans. (**A**) Consensus P2RX4 tissue expression based on datasets of HPA (Human Protein Atlas), GTEx, and FANTOM5 (function annotation of the mammalian genome). (**B**) Abundance of the P2RX4 protein in human normal tissues. Representative immunohistochemistry images of P2RX4 expression between normal (left) and tumor (right) tissues. (**C**) Breast. (**D**) Kidney. (**E**) Colon. (**F**) Cerebral cortex. (**G**) Liver. (**H**) Endometrium. scale = 200 μm (**I**) We also looked at the abundance of P2RX4 protein in normal tissues vs. primary breast cancer, clear cell RCC, colon cancer, Glioblastoma multiforme, liver hepatocellular carcinoma and UCEC tissues using the CPTAC dataset (***$p < 0.001$ vs. Normal).

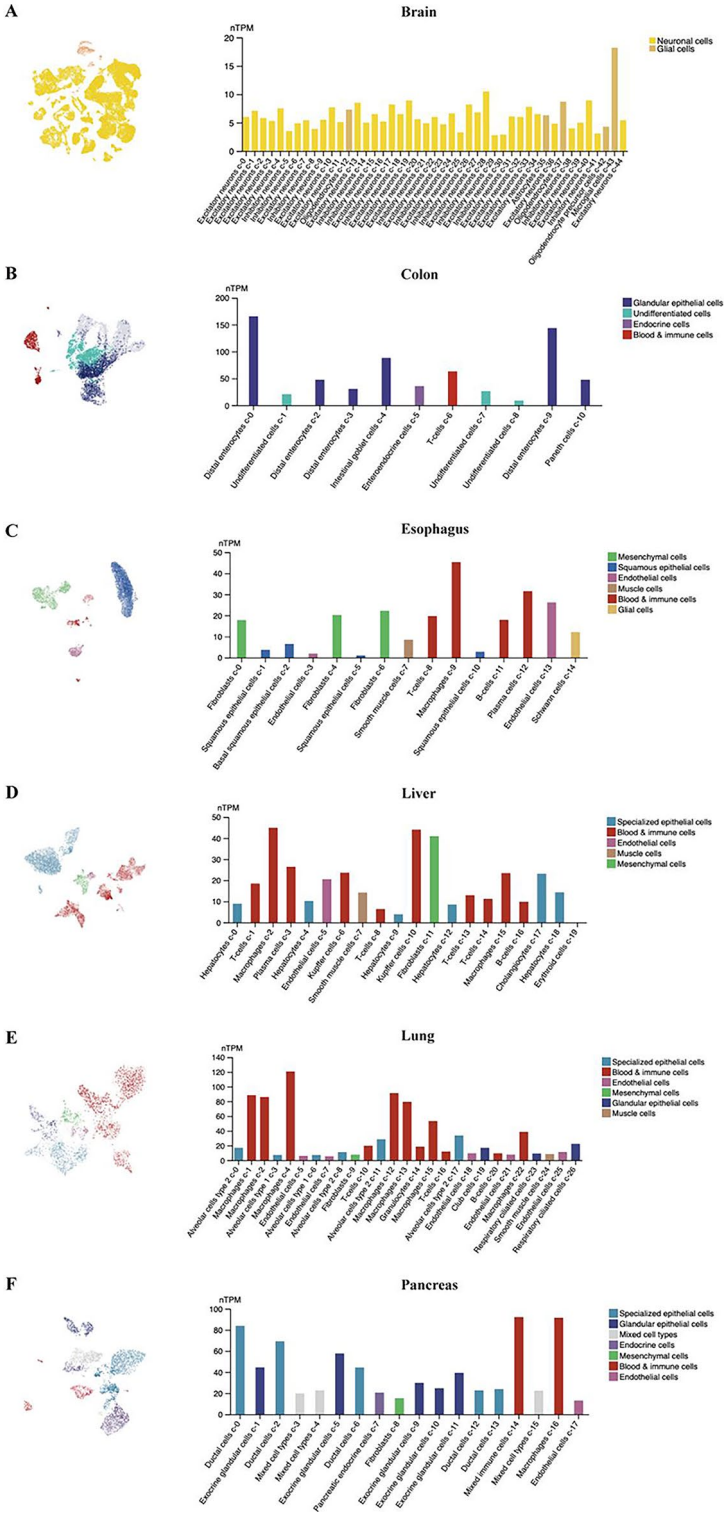

Fig. 3. (**A**–**K**) For each analyzed tissue, single cell RNA levels of defined cell type groupings. The amount of nTPM in each annotated cluster of single cells is depicted by the bar chart. On the left, the UMAP plot illustrates the RNA expression profile. Color coding is based on cell type groupings, which are composed of cell types with similar functional features. It should be noted that the same cell type may be found in numerous clusters.

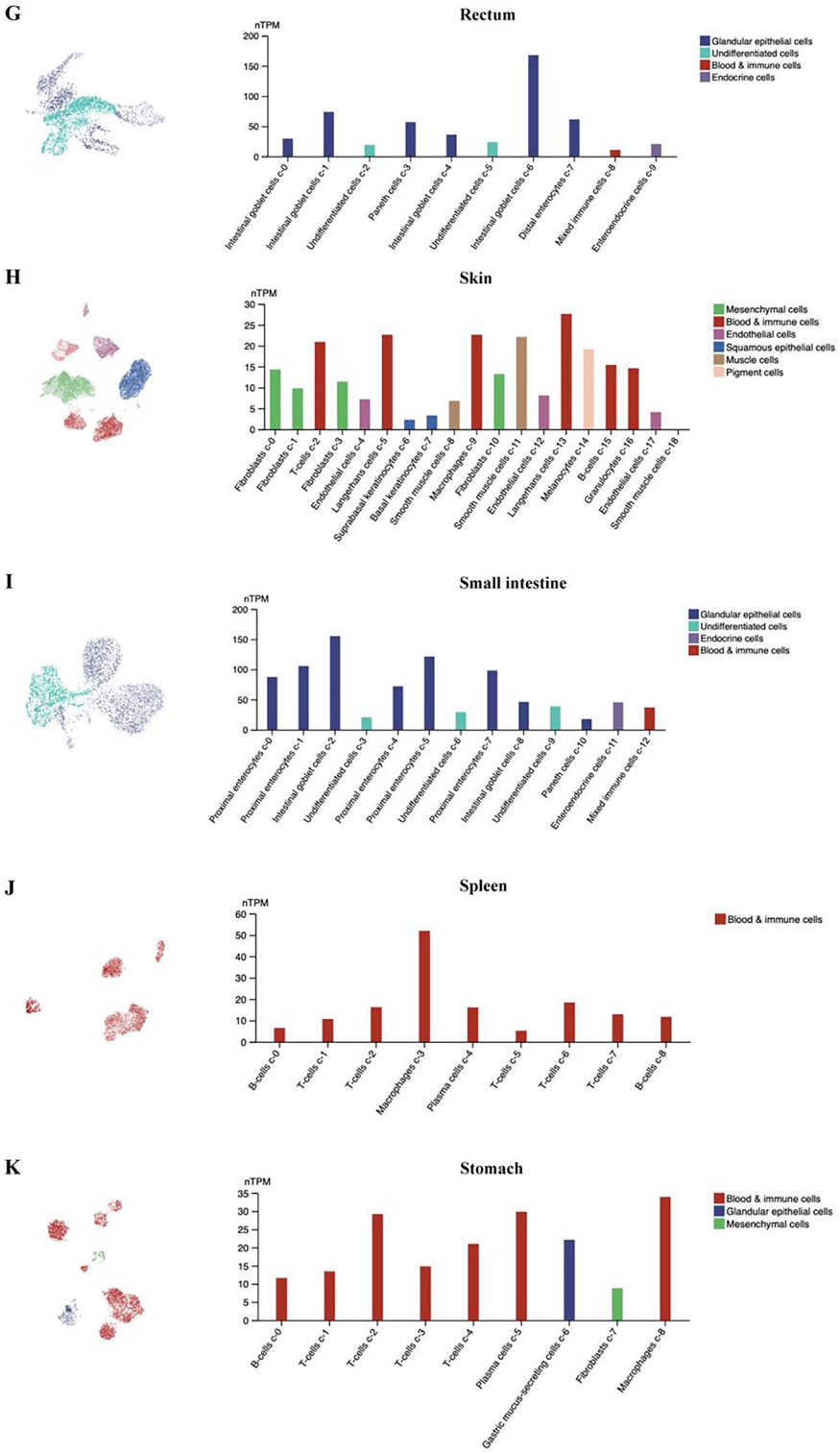

Figure 3. (continued)

Prognostic value of P2RX4 across cancer

We classified cancer cases as high-expression or low-expression based on P2RX4 expression levels and investigated the connection between P2RX4 expression level and prognosis in patients with diverse malignancies, largely using the TCGA and GEO datasets. Figure 4A showed that high expression of P2RX4 was associated with poor prognosis in terms of OS for GBM (Fig. 4B, Logrank $p = 0.01$, HR = 1.6), LGG (Fig. 4C, Logrank $p = 0.00036$, HR = 1.9), LIHC (Fig. 4D, Logrank $p = 0.029$, HR = 1.5), LUSC (Fig. 4E, Logrank $p = 0.006$, HR = 1.5), mesothelioma (MESO) (Fig. 4F, Logrank $p = 0.024$, HR = 1.7) and uveal melanoma (UVM) (Fig. 4G, Logrank

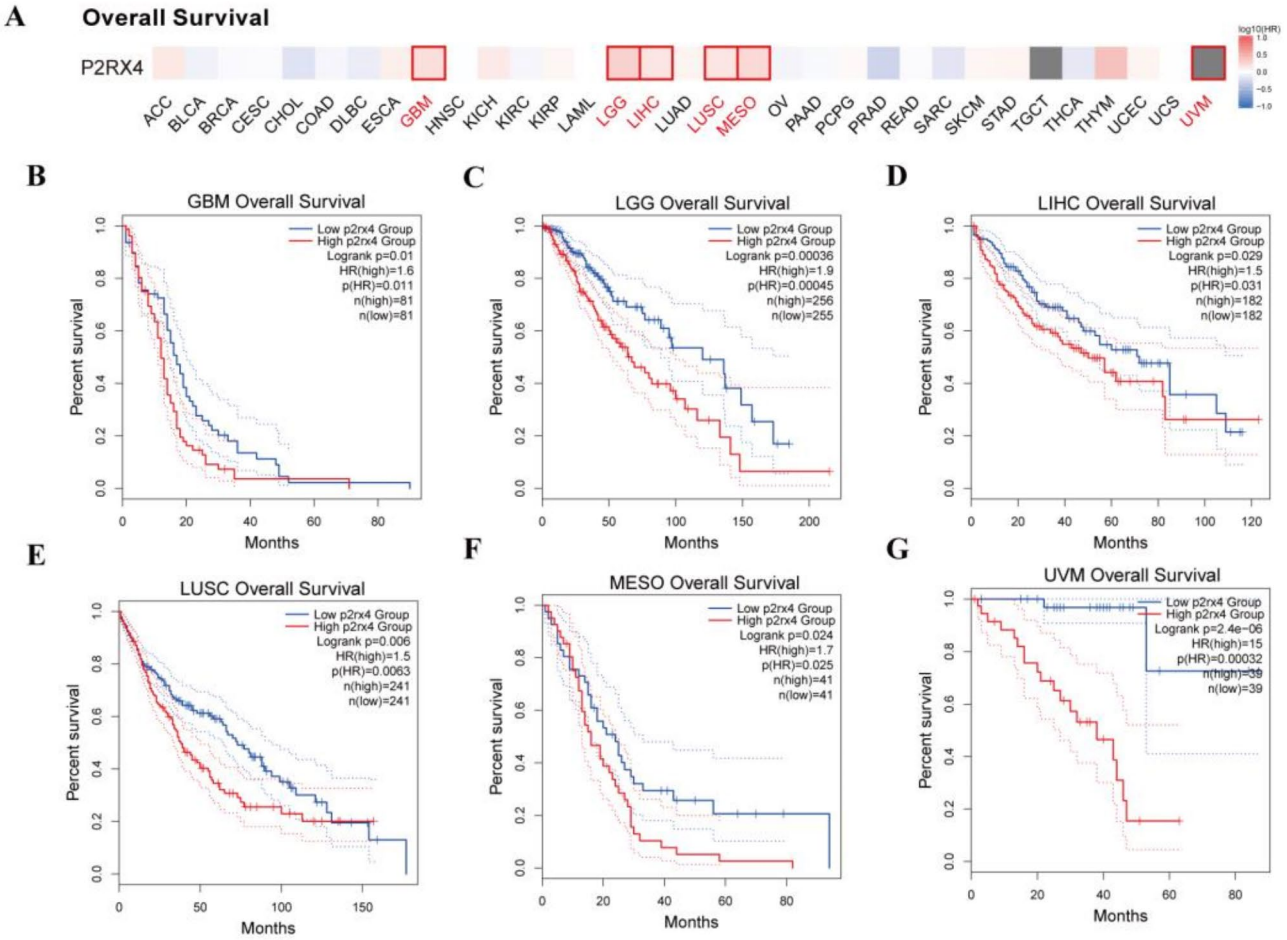

Fig. 4. P2RX4 expression and overall survival (OS) in patients with various TCGA tumor types were correlated. GEPIA2 was used to generate a survival map (**A**) and to perform overall survival analysis (**B**–**G**). With significant findings, the survival map and Kaplan-Meier plots are presented. The 95% confidence intervals of OS for high and low P2RX4 expression groups are given by red and blue dotted lines, respectively.

p = 2.4e−06, HR = 15) cancers according to TCGA data. The results of DFS analysis (Fig. 5A) demonstrated a relationship between high P2RX4 level and poor prognosis for TCGA cases of LGG (Fig. 5B, Logrank p = 0.00034, HR = 1.8), LUSC (Fig. 5C, Logrank p = 0.00025, HR = 1.9), THCA (Fig. 5E, Logrank p = 0.012, HR = 2.2) and UVM (Fig. 5F, Logrank p = 3.8e−05, HR = 8.8). Moreover, low P2RX4 level was related to a poor DFS prognosis for SARC (Fig. 5D, Logrank p = 0.033, HR = 0.68).

Diagnosis value of P2RX4 across cancers

The ROC curves were used to evaluate the effectiveness of P2RX4 diagnosis. AUC values between 0.9 and 1.0 were considered high diagnostic accuracy, and confidence intervals (CI) values between 0.7 and 0.9 were considered relative diagnostic accuracy. The AUC model had relative diagnostic accuracy in 17 kinds of cancer, including BRCA (AUC = 0.702, CI: 0.656–0.747), COAD (AUC = 0.704, CI: 0.617–0.790), UCEC (AUC = 0.705, CI: 0.611-0.800), HNSC (AUC = 0.715, CI: 0.622–0.807), ESAD (AUC = 0.719, CI: 0.494–0.943), STAD (AUC = 0.729, CI: 0.633–0.824), THCA (AUC = 0.734, CI: 0.683–0.786), CESC (AUC = 0.739, CI: 0.612–0.866), LUAD (AUC = 0.776, CI: 0.736–0.817), UCS (AUC = 0.797, CI: 0.711–0.883), ACC (AUC = 0.818, CI: 0.746–0.889), OV (AUC = 0.819, CI: 0.783–0.855), LGG (AUC = 0.852, CI: 0.834–0.870), LAML (AUC = 0.853, CI: 0.805-0.900), GBMLGG (AUC = 0.858, CI: 0.841–0.875), GBM, (AUC = 0.878, CI: 0.846–0.910) and THYM (AUC = 0.888, CI: 0.856–0.920) (Fig. S3A-Q). The model's AUC has a high diagnosis accuracy in 5 forms of cancer, including SKCM (AUC = 0.909, CI: 0.894–0.924), PAAD (AUC = 0.923, CI: 0.890–0.957), KIRC (AUC = 0.927, CI: 0.899–0.956), CHOL (AUC = 0.929, CI: 0.848-1.000) and KICH (AUC = 0.975, CI: 0.948-1.000) (Fig. S3R-V).

Mutational analysis of P2RX4

Then, we utilized cBioPortal to explore the P2RX4 mutation frequency based on the TCGA database (10967 samples from 32 studies), and observed that DLBC had a considerably high mutation rate, with the P2RX4 alteration frequency above 4% (Figs. 6A-B). The majority of genetic alterations in Mature B-Cell Neoplasms samples were homdel and mutant mutations (Supplementary Table 1), which were the most common types of genetic alteration in all TCGA tumor samples. There were 48 P2RX4 mutations found, including 37

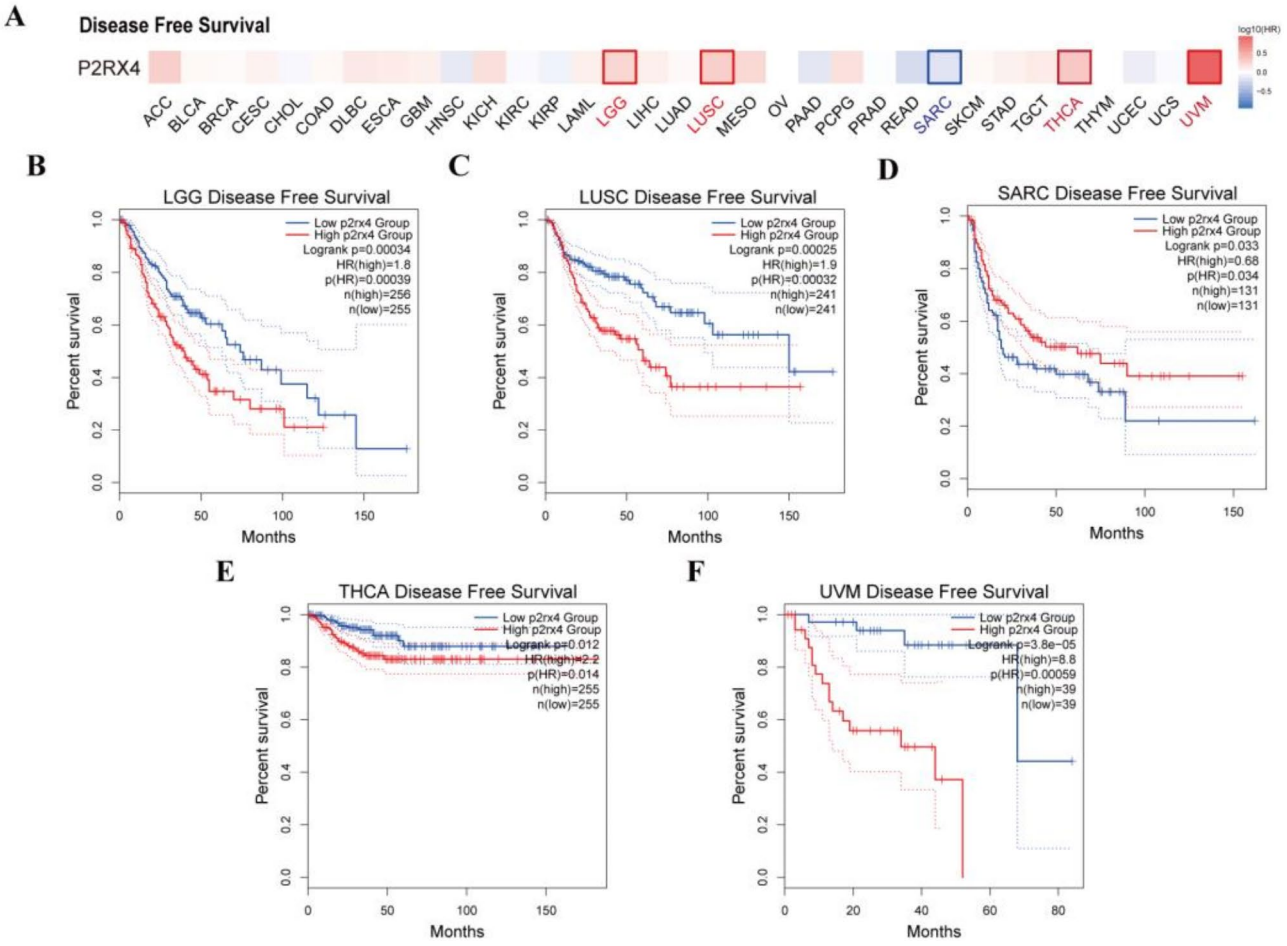

Fig. 5. The relationship between P2RX4 expression and disease-free survival (DFS) in patients with various TCGA tumor types. GEPIA2 was used to create a survival map (**A**) and to perform DFS analysis (**B**–**F**). The survival map and Kaplan-Meier plots with significant findings are shown. The 95% confidence intervals for DFS are given by red and blue dotted lines for high and low P2RX4 expression groups, respectively.

missense mutations, 4 truncating mutations, 4 splice mutations, 1 inframe mutations, and 2 sv/fusion mutation (Supplementary Table 2; Fig. 6C). A162G/V was the most typical mutation location among them.

Immune infiltration analysis

Tumor-infiltrating immune cells are linked to cancer occurrence, progression, and metastasis as essential components of the tumor microenvironment[24,25]. In the tumor microenvironment stroma, cancer-related fibroblasts are hypothesized to influence the activities of numerous tumor-infiltrating immune cells[26,27]. We found a significant negative association between immunological infiltration of CD8 + T-cells and P2RX4 expression in BRCA, THYM, and TGCT tumors, but a positive relationship for HNSC-HPV$^+$, LUSC, SARC and UVM (Figure S4A). Moreover, for the TCGA tumors ACC, BLCA, LGG, LUSC, TGCT, HNSC (HPV), THYM and UVM, there was a significant positive correlation between P2RX4 expression and the approximated infiltration value of CAF, but a negative association for BRCA-LumA, PRAD and THCA (Figure S4A). Scatterplot data for the tumors mentioned above generated by a single algorithm were shown in Figures S4B and S5B. The level of P2RX4 expression in BRCA-LumA (Rho = -0.132, $p = 2.64e{-}03$), PRAD (cor = -0.133, $p = 6.76e{-}03$) and THCA (cor = -0.142, $p = 1.62e{-}03$) was negatively linked with the extent of infiltration of CAF, according to the MCPCOUNTE algorithm (Figure S5B).

Enrichment analysis of P2RX4-related genes

To explore potential biological functions of P2RX4, we applied GEPIA2 to screen the top 100 common expressed genes (Supplementary Table 3). These genes functional analyses on the Metascape website revealed that they were closely connected to autophagy, protein modification (unfolded protein and glycosylation), or intracellular trafficking (Golgi and zinc ion; Fig. 7A). We found 48 proteins interacting with P2RX4 through BioGRID (Supplementary Table 4), with SPPL2B, EIF2B1, EIF2B2, EIF2B3, EIF2B4 and EIF2B5 being closer (Fig. 7B). These proteins participated in the biosynthesis of cellular macromolecules, transmembrane proteolysis and protein translation (Supplementary Table 5)[28,29]. Additionally, P2RX4 expression was intimately linked to

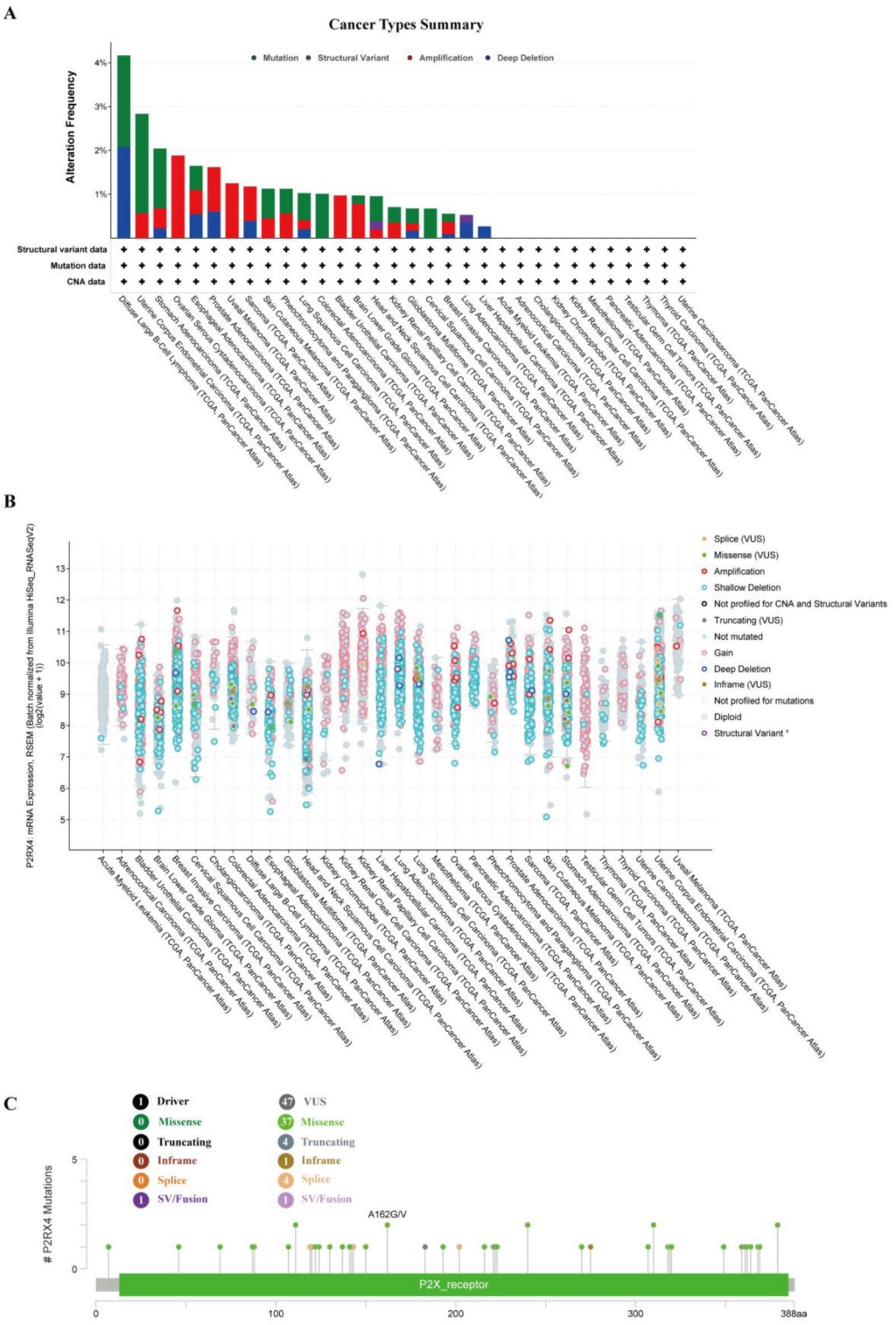

Fig. 6. P2RX4 mutation landscape. (**A**) P2RX4 mutation frequency in multiple TCGA pan-cancer studies according to the cBioPortal database. (**B**) General mutation count of P2RX4 in various TCGA cancer types according to the cBioPortal database. (**C**) Mutation diagram of P2RX4 in different cancer types across protein domains.

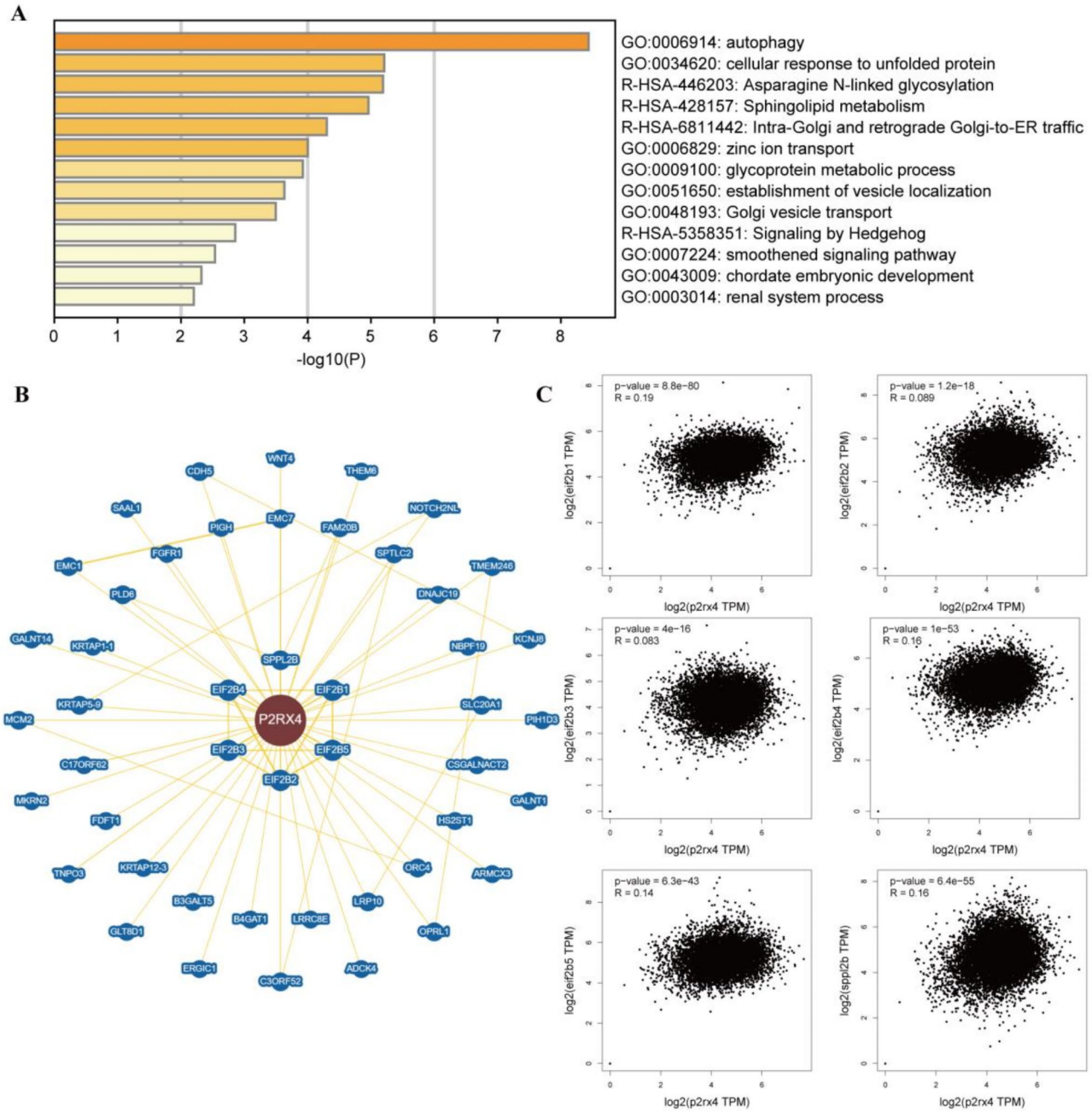

Fig. 7. Analysis of P2RX4-related gene enrichment. (**A**) Gene Ontology analysis of the top 100 genes co-expressed with P2RX4. (**B**) BioGRID-derived P2RX4-protein interactions. (**C**) GEPIA2 performed a correlation study of P2RX4 and SPPL2B, EIF2B1, EIF2B2, EIF2B3, EIF2B4 and EIF2B5 across all tumor samples in the TCGA.

SPPL2B, EIF2B1, EIF2B2, EIF2B3, EIF2B4 and EIF2B5 expression levels (Fig. 7C). P2RX4 may promote cancer via activating autophagy, protein modification, translation or intracellular trafficking, according to these studies.

P2RX4 expression in LIHC

We examined the protein levels and gene levels of 5 pairs of LIHC tissues and neighboring normal tissue samples in the clinic to confirm the expression of P2RX4 in LIHC. To begin, P2RX4 protein expression was measured in 5 pairs of tissues and found to be considerably higher in LIHC than in normal tissues (Fig. 8A-B). Furthermore, P2RX4 gene expression was considerably higher in the 5 groups of LIHC tissues compared to the control group (Fig. 8C).

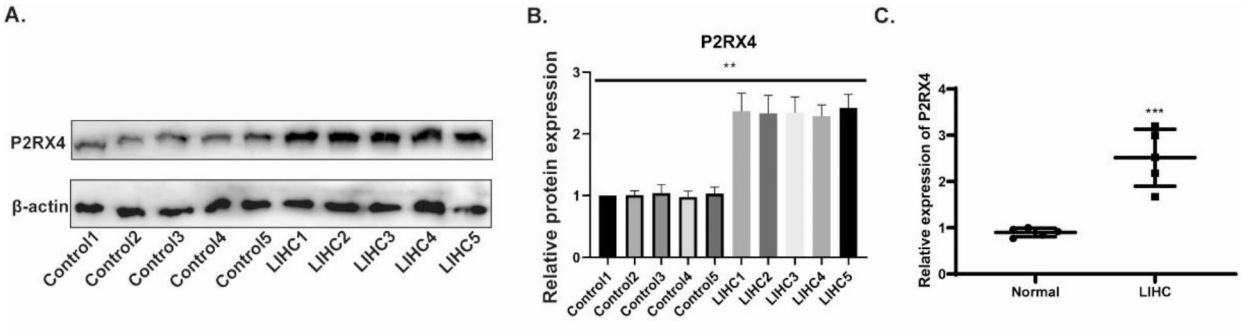

Fig. 8. Analysis of the expression level of P2RX4 in liver hepatocellular carcinoma. (**A**,**B**) Examination of P2RX4 protein expression levels by Western blot. (**B**) Detection of P2RX4 gene expression levels by Real-time Quantitative PCR (RT-qPCR). * $P<0.05$, ** $P<0.01$, *** $P<0.001$ vs. Control/Normal.

Silencing of P2RX4 suppresses cell viability, migration and invasion of U251 and PC3

Astrocytes HEB and glioblastoma cells U251 were cultured in vitro. The expression level of P2RX4 in these cells was detected by Western blot and RT-qPCR, which demonstrated that compared with HEB cells, U251 cells exhibited significantly elevated P2RX4 expression levels (Fig. 9A). Similarly, in normal prostate cells RWPE-1 and prostate cancer cells PC3 cultured in vitro, P2RX4 expression was markedly higher in PC3 cells compared to RWPE-1 cells (Fig. 9B). To investigate functional consequences, P2RX4 expression was knocked down in U251 and PC3 cells through cell transfection. The knockdown efficiency was confirmed by Western blot, which verified successful reduction of P2RX4 expression in both cell lines (Fig. 9C). CCK-8 assay showed substantially reduced proliferative capacity in si-P2RX4 groups compared to si-NC controls (Fig. 9D). Flow cytometry revealed significantly increased apoptosis rates in P2RX4-deficient cells (Fig. 9F). ELISA detection indicated elevated intracellular ROS levels in si-P2RX4 group compared with si-NC group (Fig. 9E). Wound healing and Transwell assays demonstrated markedly impaired migration and invasion capabilities in si-P2RX4 treated cells relative to the si-NC group (Fig. 9G-H).

Discussion

Cancer study has long been a research priority in the modern medical realm. Breast, lung, and colon cancer are the three most frequent malignancies globally[1]. Through gene expression difference analysis, 33 cancer-associated data from the TCGA and GTEx databases were utilized to investigate biomarkers appropriate for broad-spectrum cancer detection. Through comprehensive pan-cancer analysis, this study revealed that P2RX4 exhibited aberrant overexpression in multiple malignancies, correlated with poor prognosis, and modulated tumor immunity and cellular processes such as autophagy.

Our analysis demonstrated that P2RX4 was significantly upregulated in 19 tumor types, including LIHC, GBM, and BRCA, and its overexpression predicted unfavorable OS and DFS in cancers such as LGG, UVM, and LUSC. These findings align with prior studies reporting elevated P2RX4 levels in hepatobiliary carcinoma and glioma[30–32]. The diagnostic potential of P2RX4 was further underscored by its high AUC values in SKCM, PAAD, and KICH, suggesting its utility as a broad-spectrum biomarker. The consistency between TCGA, CPTAC, and IHC data reinforced the reliability of these observations. Mechanistically, P2X receptors may act as an oncogene by promoting tumor cell survival and proliferation, potentially through its ATP-gated ion channel activity, which regulates calcium influx and downstream signaling pathways[33]. Moreover, we discovered that the protein levels and gene expression levels of P2RX4 were considerably higher than those of the Normal group by examining the protein expression and gene expression levels of five pairs of clinically selected LIHC and normal tissues, which was consistent with the results of the previous analysis. Calphostins trigger apoptosis in breast and cervical cancer cell lines through a P2RX4-dependent elevation of intracellular calcium levels[34]. Hong et al. establish a zinc metabolism-related genes signature, encompassing P2RX4, serving as a tool for BRCA prognosis prediction[35]. Moreover, P2RX4 demonstrates high expression in glioma cells, with its silencing hindering cell viability and proliferation by curbing the BDNF/TrkB/ATF4 signaling pathway[30]. Consistent with previous studies, herein, functional assays have revealed that knocking down P2RX4 significantly inhibited the malignant progression of GBM and prostate cancer cells, further demonstrating the oncogenic role of P2RX4 in various types of cancer.

Furthermore, an important finding was the positive correlation between P2RX4 expression and immune infiltration, particularly with CAFs and CD8 + T cells in tumors such as ACC, LUSC, and UVM. CAFs are known to remodel the extracellular matrix, secrete pro-tumorigenic cytokines, and suppress anti-tumor immunity[26,36]. The association of P2RX4 with CAF infiltration implies its role in fostering a tumor-permissive stroma. Conversely, the negative correlation in BRCA-LumA and PRAD suggests context-dependent interactions, possibly influenced by hormonal signaling or tumor subtype-specific microenvironments. The four-gene (PTPN12, IDH2, P2RX4, and KDELR2) prognostic risk model established by Wang et al. promotes the infiltration of CD8 + T cells in uveal melanoma through antigen presentation, leading to an unfavorable prognosis[37]. Therefore, P2RX4 plays a role in modulating tumor immunity and the microenvironment.

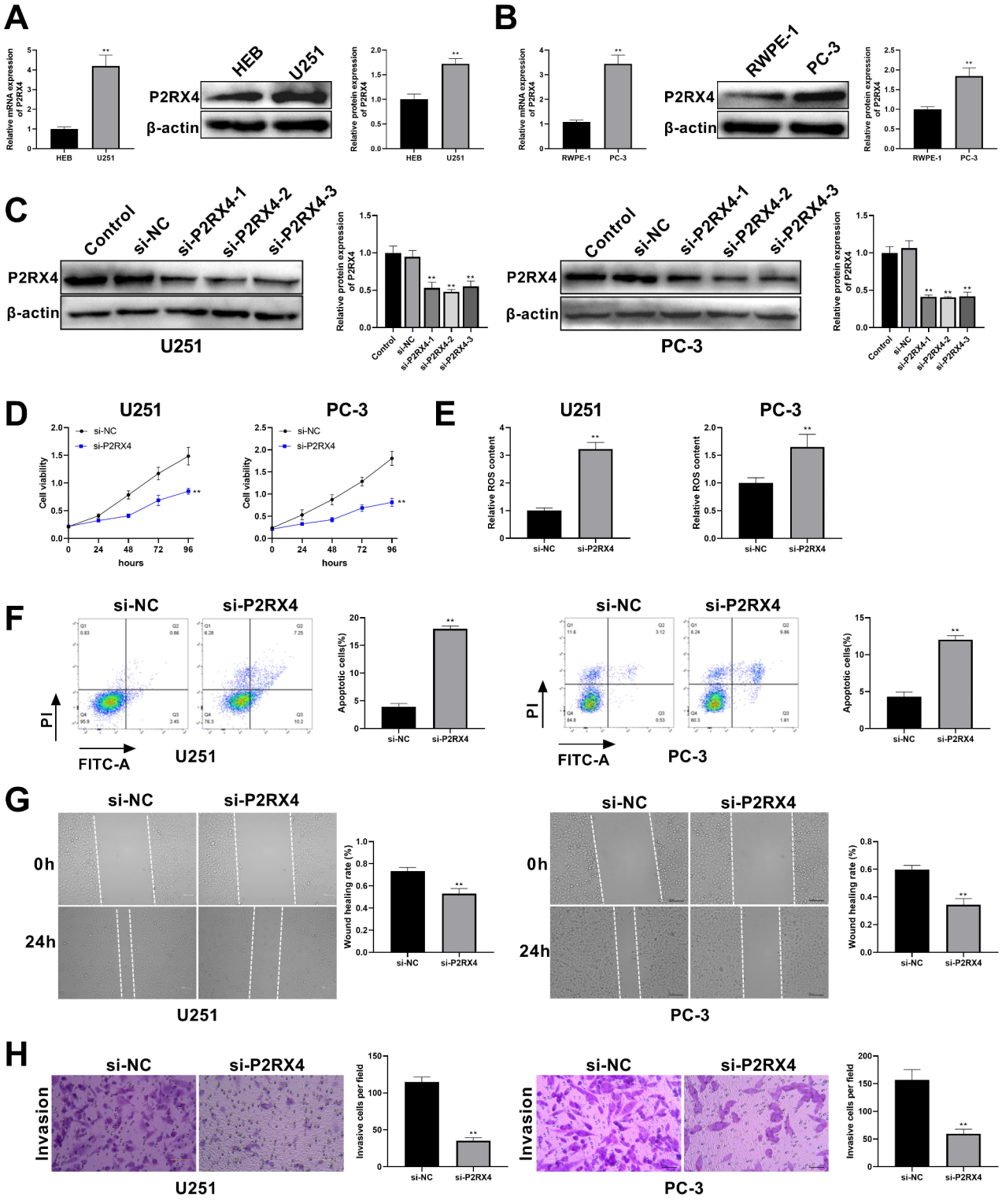

Fig. 9. (**A**) The expression of P2RX4 in astrocytes and glioblastoma cells was determined by RT-qPCR and Western blot. ** $P<0.01$ vs. HEB. (**B**) The expression of P2RX4 in normal prostate cells and prostate cancer cells was assessed using RT-qPCR and Western blot. ** $P<0.01$ vs. RWPE-1. (**C**) The knockdown efficiency of P2RX4 in U251 and PC3 cells was evaluated by Western blot. (**D**) Cell viability was measured using the cell counting kit-8 assay. (**E**). Reactive oxygen species level was quantified through Enzyme-Linked Immunosorbent Assay. (**F**) Cell apoptosis was analyzed by flow cytometry. (**G**) Cell migration was examined with the wound healing assay. (**H**) Cell invasion was assessed via the Transwell assay. **$P<0.01$ vs. si-NC.

Applying GEPIA2, we uncovered a slew of genes that co-expressed with P2RX4 in a variety of cancers. Enrichment analysis revealed that P2RX4-associated genes were involved in autophagy, protein modification, and intracellular trafficking. Autophagy, a double-edged sword in cancer, can either suppress tumor initiation or promote survival under stress[38]. P2RX4 may drive tumor progression by sustaining autophagy-mediated nutrient recycling, as evidenced in BRCA models[13]. Furthermore, through using BioGRID database, we identified 48 proteins that physically interact with P2RX4. The expression of SPPL2B, EIF2B1, EIF2B2, EIF2B3, EIF2B4 and EIF2B5 is intimately linked to the expression of P2RX4. SPPL2B, EIF2B1, EIF2B2, EIF2B3, EIF2B4 and EIF2B5 are well-studied cellular macromolecule biosynthesis processes, as are transmembrane proteolysis and protein translation[39,40]. These pathways could synergize with P2RX4's ion channel activity to enhance tumor cell adaptability and metastatic potential.

The present investigation, however, has certain drawbacks. For starters, the sample size for numerous uncommon tumor types was small, which might have resulted in batch effects or incorrect results. Second, while bioinformatics tools like TIMER2 and cBioPortal provide robust preliminary insights, in vivo models and mechanistic studies are required to confirm P2RX4's role in autophagy and immune infiltration. In addition, the clinical relevance of P2RX4 mutations warrants investigation into their prognostic and predictive value across diverse cohorts. Future work should prioritize functional assays across diverse cancer types to validate these findings.

To recapitulate, we revealed that P2RX4 was extensively differently expressed across tumor tissues and normal tissues using pan-cancer analysis and discovered a link between P2RX4 expression and clinical prognosis. P2RX4 emerged as a multifaceted regulator of tumor progression, influencing immune evasion, stromal interactions, and stress adaptation. Its pan-cancer overexpression and prognostic significance positioned it as a promising biomarker and therapeutic target. Future research should prioritize functional validation and translational studies to harness P2RX4's potential in precision oncology.

Data availability

The datasets analysed during the current study are available in the TIMER2 database (http://timer.cistrome.org/), the Cancer Genome Atlas database (TCGA; https://www.cancer.gov/ccg/research/genome-sequencing/tcga) and the HPA database (http://www.proteinatlas.org/).

Received: 5 August 2024; Accepted: 19 March 2025
Published online: 03 April 2025

References

1. Sung, H. et al. Global cancer statistics 2020: GLOBOCAN estimates of incidence and mortality worldwide for 36 cancers in 185 countries. *CA Cancer J. Clin.* **71** (3), 209–249 (2021).
2. Bray, F. et al. Global cancer statistics 2022: GLOBOCAN estimates of incidence and mortality worldwide for 36 cancers in 185 countries. *CA Cancer J. Clin.* **74** (3), 229–263 (2024).
3. Singh, A. K. & McGuirk, J. P. CAR T cells: continuation in a revolution of immunotherapy. *Lancet Oncol.* **21** (3), e168–e178 (2020).
4. Liu, B. et al. Identification of DRP1 as a prognostic factor correlated with immune infiltration in breast cancer. *Int. Immunopharmacol.* **89(Pt B)**, p107078 (2020).
5. Hu, A. et al. Pan-cancer analysis reveals DDX21 as a potential biomarker for the pro gnosis of multiple tumor types. *Front. Oncol.* **12**.
6. Ulmann, L., Hirbec, H. & Rassendren, F. P2X4 receptors mediate PGE2 release by tissue-resident macrophages and initiate inflammatory pain. *Embo J.* **29** (14), 2290–2300 (2010).
7. Ulmann, L. et al. Up-regulation of P2X4 receptors in spinal microglia after peripheral nerve injury mediates BDNF release and neuropathic pain. *J. Neurosci.* **28** (44), 11263–11268 (2008).
8. Tsuda, M. et al. P2X4 receptors induced in spinal microglia gate tactile allodynia after nerve injury. *Nature* **424** (6950), 778–783 (2003).
9. Ledderose, C. et al. Purinergic P2X4 receptors and mitochondrial ATP production regulate T cell migration. *J. Clin. Invest.* **128** (8), 3583–3594 (2018).
10. Yang, T. et al. Novel protective role of endogenous cardiac myocyte P2X4 receptors in heart failure. *Circ. Heart Fail.* **7** (3), 510–518 (2014).
11. Zhang, P. A. et al. Overexpression of Purinergic P2X4 Receptors in Hippocampus Rescues Memory Impairment in Rats with Type 2 Diabetes. *Neurosci. Bull.* **36** (7), 719–732 (2020).
12. Maynard, J. P. et al. P2X4 purinergic receptors offer a therapeutic target for aggressive prostate cancer. *J. Pathol.* **256** (2), 149–163 (2022).
13. Chadet, S. et al. P2x4 receptor promotes mammary cancer progression by sustaining autophagy and associated mesenchymal transition. *Oncogene* **41** (21), 2920–2931 (2022).
14. Tien, F. M. et al. Epigenetic remodeling of the immune landscape in cancer: therapeutic hurdles and opportunities. *J. Biomed. Sci.* **30** (1), 3 (2023).
15. Sanchez-Vega, F. et al. Oncogenic signaling pathways in the cancer genome atlas. *Cell* **173** (2), 321–337e10 (2018).
16. Liu, M. C. et al. Sensitive and specific multi-cancer detection and localization using methylation signatures in cell-free DNA. *Ann. Oncol.* **31** (6), 745–759 (2020).
17. Li, T. et al. TIMER2.0 for analysis of tumor-infiltrating immune cells. *Nucleic Acids Res.* **48** (W1), W509–w514 (2020).
18. Tang, Z. et al. GEPIA2: an enhanced web server for large-scale expression profiling and interactive analysis. *Nucleic Acids Res.* **47** (W1), W556–w560 (2019).
19. Chandrashekar, D. S. et al. UALCAN: an update to the integrated cancer data analysis platform. *Neoplasia* **25**, 18–27 (2022).
20. Pontén, F. et al. The human protein atlas as a proteomic resource for biomarker discovery. *J. Intern. Med.* **270** (5), 428–446 (2011).
21. Gao, J. et al. Integrative analysis of complex cancer genomics and clinical profiles using the cBioPortal. *Sci. Signal.* **6** (269), pl1 (2013).
22. Zhou, Y. et al. Metascape provides a biologist-oriented resource for the analysis of systems-level datasets. *Nat. Commun.* **10** (1), 1523 (2019).
23. Oughtred, R. et al. The biogrid database: A comprehensive biomedical resource of curated protein, genetic, and chemical interactions. *Protein Sci.* **30** (1), 187–200 (2021).

24. Fridman, W. H. et al. Immune infiltration in human cancer: prognostic significance and disease control. *Curr. Top. Microbiol. Immunol.* **344**, 1–24 (2011).
25. Steven, A. & Seliger, B. The role of immune escape and immune cell infiltration in breast cancer. *Breast Care (Basel).* **13** (1), 16–21 (2018).
26. Chen, X. & Song, E. Turning foes to friends: targeting cancer-associated fibroblasts. *Nat. Rev. Drug Discov.* **18** (2), 99–115 (2019).
27. Kwa, M. Q., Herum, K. M. & Brakebusch, C. Cancer-associated fibroblasts: how do they contribute to metastasis? *Clin. Exp. Metastasis.* **36** (2), 71–86 (2019).
28. Ballin, M. et al. *The intramembrane proteases SPPL2a and SPPL2b regulate the homeostasis of selected SNARE proteins.* Febs j, (2022).
29. Martin, L., Fluhrer, R. & Haass, C. Substrate requirements for SPPL2b-dependent regulated intramembrane proteolysis. *J. Biol. Chem.* **284** (9), 5662–5670 (2009).
30. Huo, J. F. & Chen, X. B. P2X4R silence suppresses glioma cell growth through BDNF/TrkB/ATF4 signaling pathway. *J. Cell. Biochem.* **120** (4), 6322–6329 (2019).
31. Chong, J. H. et al. Abnormal expression of P2X family receptors in Chinese pediatric acute leukemias. *Biochem. Biophys. Res. Commun.* **391** (1), 498–504 (2010).
32. Asif, A. et al. Role of purinergic receptors in hepatobiliary carcinoma in Pakistani population: an approach towards proinflammatory role of P2X4 and P2X7 receptors. *Purinergic Signal.* **15** (3), 367–374 (2019).
33. Nie, X. H., Li, T. Z. & Peng, C. M. ATP ion channel-type P2X purinergic receptors as a key regulatory molecule in breast cancer progression. *Pathol. Res. Pract.* **267**, 155844 (2025).
34. Neha, P., Ranjan & Das, P. Calcimycin mediates apoptosis in breast and cervical cancer cell lines by inducing intracellular calcium levels in a P2RX4-dependent manner. *Biochim. Biophys. Acta Gen. Subj.* **1868** (2), 130535 (2024).
35. Hong, J. et al. A zinc metabolism-related gene signature for predicting prognosis and characteristics of breast cancer. *Front. Immunol.* **14**, 1276280 (2023).
36. Calon, A. et al. Stromal gene expression defines poor-prognosis subtypes in colorectal cancer. *Nat. Genet.* **47** (4), 320–329 (2015).
37. Zhang, C. et al. Identification of co-expressed gene networks promoting CD8(+) T cell infiltration and having prognostic value in uveal melanoma. *BMC Ophthalmol.* **23** (1), 354 (2023).
38. Russell, R. C. & Guan, K. L. The multifaceted role of autophagy in cancer. *Embo J.* **41** (13), e110031 (2022).
39. Mentrup, T. et al. Physiological functions of SPP/SPPL intramembrane proteases. *Cell. Mol. Life Sci.* **77** (15), 2959–2979 (2020).
40. Wortham, N. C. & Proud, C. G. eIF2B: recent structural and functional insights into a key regulator of translation. *Biochem. Soc. Trans.* **43** (6), 1234–1240 (2015).

Author contributions

Conceptualization, XYQ; Data curation, CYW; Formal analysis, XYQ and CYW; Funding acquisition, XYQ; Methodology, XYQ and CYW; Supervision, JM; Writing-original draft, XYQ; Writing-review and editing, CYW and JM. All authors read and approved the final version of the manuscript.

Funding

This study was supported by Fundamental Research Program of Shanxi Province (No.202203021212066), Four "Batches" Innovation Project of Invigorating Medical through Science and Technology of Shanxi Province (2022XM07) and Medical Key Science Project of Shanxi Province (No. 2020XM52).

Declarations

Competing interests

The authors declare no competing interests.

Ethics approval

All methods were carried out in accordance with relevant guidelines and regulations. All experimental protocols were approved by the Ethics Committee of Shanxi Cancer Hospital following Declaration of Helsinki. And informed consent was obtained from all subjects and their legal guardian.

Additional information

Supplementary Information The online version contains supplementary material available at https://doi.org/10.1038/s41598-025-95247-9.

Correspondence and requests for materials should be addressed to J.M.

Reprints and permissions information is available at www.nature.com/reprints.

Publisher's note Springer Nature remains neutral with regard to jurisdictional claims in published maps and institutional affiliations.